Run-15 J/ψ, $\psi(2s) \rightarrow \mu^+\mu^-$ with the FVTX

J. Matthew Durham for the LANL group

September 12, 2015

1 Introduction

This Note describes a measurement of the ratio of $\psi(2s)/\psi(1s)$ mesons at forward rapidity, through their decays to dimuons, from the Run-15 $p + p$, p+Al, and p+Au data. All analysis techniques (cuts, corrections, and fitting routines) are identical between the three datasets unless explicitly stated otherwise.

The analysis proceeds as follows: First, the dimuon invariant mass spectrum is prepared using tracks that are measured in the muon arms that are matched to the FVTX. The fully refitted track including FVTX information is used to find the invariant mass of muon pairs. The ROOT likelihood fitter is then used to fit the invariant mass spectrum with a sum of combinatorial background, correlated background, and two peaks which represent the $\psi(1s)$ and $\psi(2s)$ charmonium states. The integrals of these peak shapes are extracted from the fit. These integrals are corrected for differences in detector acceptance between the two states, and the ratio $\psi(2s)/\psi(1s)$ is determined, where many systematic uncertainties cancel. For comparisons between $p + p$ and p+A data, the ratio of the ratio between 2s and 1s states in p+A to $p + p$ is calculated, where the acceptance and efficiency corrections in the detector cancel. Remaining systematic uncertainties are determined by varying the peak shapes and background normalization.

Dimuon Mass

2 Dimuon Mass

The mass of each dimuon pair is calculated using a fully refitted track that includes a MuID road with hits in the MuTracker and FVTX. Since the FVTX is located in front of the hadron absorber, the FVTX measures the muon pair opening angle before any multiple scattering in the absorber material takes place. This location, combined with the small strip size in the FVTX, gives a far superior measurement of pair opening angle (and therefore mass) than is possible with the muon tracking chambers alone.

Muon track candidates are identified using the muon arm cuts given in Tab. 1. To be considered in this analysis, tracks must reach at least the third gap in the MuID, have a good match with a MuID road, and have a reasonable chi2 value in the muon arm. Additionally, tracks that form a pair are required to pass through different octants, as typically occurs for actual charmonia dimuon decays.

Additional requirements from the FVTX further constrain the tracks and reject background, and are summarized in Tab. 2. Track matching between the FVTX and MuTr is considered in the three polar coordinates r, θ, and ϕ. As the deflection due to multiple scattering in the absorber is highly dependent on muon momentum, these cuts are sigmalized in p, and we require matching within 5σ.

In addition, events are required to have a vertex position as determined by the FVTX within 40 cm of the nominal vertex position, and events are required to have fired to 2D dimuon trigger.

Variable	Accepted Value
lastgap	>=3
DG0	$< 5\sigma$
DDG0	$< 5\sigma$
trchi2	< 23
octant cut	applied
nidhits	> 14
p_z	> 2 GeV

Table 1: Muon arm cuts (not including the FVTX).

Variable	Accepted Value
dphi_fvtx	$< 5\sigma$
dr_fvtx	$< 5\sigma$
dtheta_fvtx	$< 5\sigma$
chi2_fvtx	< 10
chi2_fvtxmutr	< 10

Table 2: FVTX cuts.

3 Acceptance $\times$ Efficiency Corrections

The dimuon acceptance and detection efficiency is a function of the pair's mass and momentum. Previous studies of the dimuon continuum for PPG154 have shown that the acceptance $\times$ efficiency of the PHENIX muon arms as a function of mass rises between 2 and 4 GeV/c^2, which indicates that this correction does NOT completely cancel out when making the $\psi(2s)/\psi(1s)$ ratio. Therefore the measured ratio must be corrected by the ratio of the acc$\times$eff value evaluated at the masses of the two particles.

The corrections used for the Run-15 preliminary result described herein are the same as were used for the Run-13 preliminary result, as described in AN1185. For details please see AN1885 Section 4. Here we use the same correction factors but, as a conservative estimate, the systematic uncertainty is doubled to 2% to account for any differences in the Run-13 and Run-15 acceptance. We note that this is not the dominant uncertainty, so even if this systematic is underestimated, it is a subdominant effect that will not change the physics interpretation of the result..

4 Combinatorial Backgrounds

Two standard methods were investigated to determine the magnitude of the uncorrelated backgrounds under the ψ and ψ' peaks in the dimuon invariant mass spectrum: the like-sign method, which uses pairs of muons with the same charge produced in an event, and the mixed event method, which constructs pairs from muons produced in different events that have similar characteristics.

4.1 Like-sign Background

Using events which satisfied the same cuts used to find the unlike-sign dimuon invariant mass spectrum, the like-sign invariant mass spectrum was found for $\mu^+\mu^+$ and $\mu^-\mu^-$ pairs. The like-sign mass spectrum is normalized following the standard PHENIX methods:

$$Normalization_{ls} = \frac{2\sqrt{N_{++}N_{--}}}{N_{++}+N_{--}} \tag{1}$$

4.2 Mixed Event Backgrounds

To overcome the statistical limitations of the like-sign background subtraction methods, we use event mixing to construct a mass spectrum of muon pairs using muons produced in different events. The contributions to the spectrum are purely combinatorial, and can have no contributions from correlated dimuon emission. Following the methods used in PPG142/AN890 (where they had a similar problem with a low statistics like-sign background), the mixed events are normalized to the like-sign by the factor:

$$Normalization_{mixed} = \frac{2\sqrt{N_{++}N_{--}}}{N_{+-}^{mix}} \tag{2}$$

where N_{+-}^{mix} is the number of unlike-sign pairs from the mixed events. A systematic uncertainty from this normalization factor is determined by varying the mass range over which the factor is calculated, see the section on systematic uncertainties and the related discussion for details.

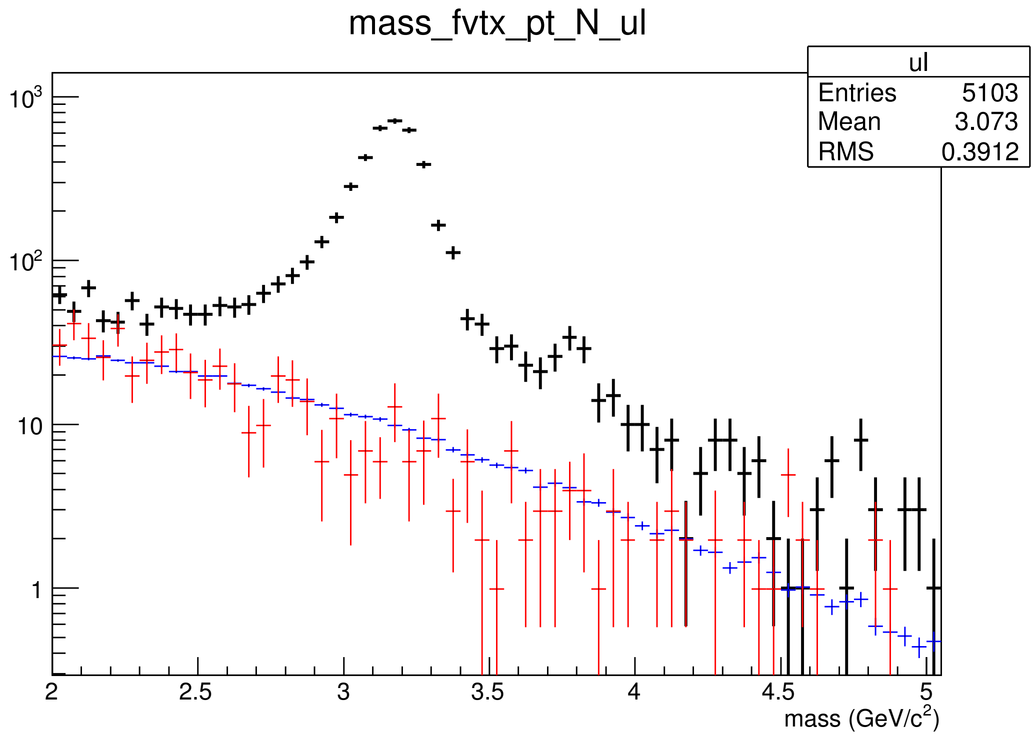

Figure 1: The unlike-sign p+Au dimuon mass spectra for the north arm (black), with two estimations of the combinatorial background, from like-sign events in red and mixed events in blue.

5 Peak Extraction

After the dimuon mass spectrum is prepared with the cuts described previously, a fit to the raw unlike-sign counts is used to extract the peaks corresponding to the $\psi(1s)$ and $\psi(2s)$ states. The total fit function includes the properly normalized mixed event combinatorial background, an exponential function to represent the correlated background dimuons, and peaks to represent the resonances. Each of the signal peaks is represented by the sum of a Gaussian and a Crystal Ball function (which itself is a Gaussian core with a power law tail to the low side that accounts for muon pairs that are reconstructed with an erroneously low mass due to range straggling in the absorber).

The Crystal Ball function is explained pretty well here:
$https://www.jlab.org/primex/weekly\_meetings/slides\_2009\_07\_17/dmitry/crystalball.html$
The fit parameters are defined as follows:

p0 - Crystal Ball parameter α,
p1 - Crystal Ball parameter n,
p2 - $\psi(1s)$ Crystal Ball parameter μ,
p3 - $\psi(1s)$ Crystal Ball parameter σ,
p4 - $\psi(1s)$ Crystal Ball parameter N,
p5 - Gaussian parameter N,
p6 - $\psi(2s)$ Crystal Ball parameter N,
p7 - Exponential background normalization,
p8 - Exponential background slope

There are several constraints on the fit function. Since both resonance peaks are expected to display similar effects from straggling in the absorber, the Crystal Ball parameters α and n which define the low mass tail are set to be the same. The width of the $\psi(2s)$ peak is expected to be wider than the $\psi(1s)$ peak, due to the fact that the higher mass and harder p_T spectrum of the 2s state will produce higher momentum decay muons, which have a larger uncertainty in reconstructed momentum in the spectrometer. The ratio of widths of the $\psi(2s)$ to $\psi(1s)$ is set to be 1.15 and varied to determine a systematic uncertainty (see following section and related discussion). The centroid of the $\psi(1s)$ peak is allowed to float. However, the difference between the centroids of the $\psi(2s)$ and $\psi(1s)$ peaks is set to the PDG value of 589 MeV/c^2 multiplied by the ratio of the value of the $\psi(1s)$ centroid from the fit to the PDG value of the $\psi(1s)$ mass . In practice, the difference in the fitted $\psi(1s)$ mass and the PDG value is 1-2%. Changing the difference between the peaks this much makes a negligibly small change in the ratio of the two states, but should correct for any errors in the magnetic field map.

The second gaussian under each peak is set to be centered at the same mass as the Crystal Ball function. The relative normalization of the second gaussian to the Crystal Ball function is set to be the same for both resonances, since they should have the same line shape. The width of the second gaussian is set to 200 MeV in the nominal fit case, and varied to determine a systematic uncertainty (see the following section and related discussion). This is the dominant contribution to the total systematic uncertainty on the ratio.

The mass distributions for the p_T-integrated dimuon sample prepared with the cuts previously discussed are shown in Figs 2 through 7 for the North and South arm of the $p+p$, $p+$Al, and $p+$Au datasets, with fits. The relevant quantities extracted from the fits are summarized in Table 3. The North and South arm $p+p$ data points are shown in Fig 8.

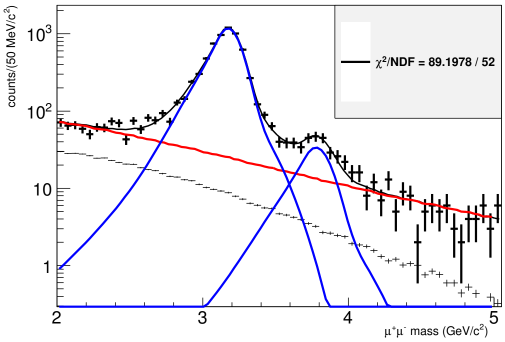

Figure 2: The unlike-sign $p+p$ dimuon mass spectra for the North arm prepared using the cuts described.

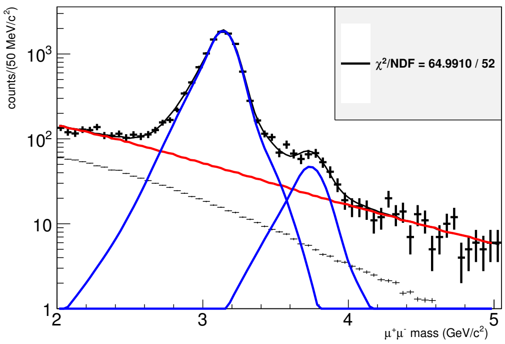

Figure 3: The unlike-sign $p+p$ dimuon mass spectra for the South arm prepared using the cuts described.

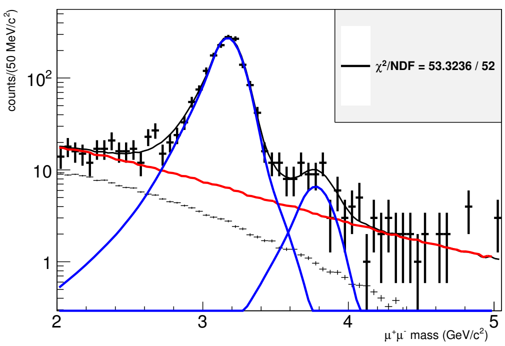

Figure 4: The unlike-sign p+Al dimuon mass spectra for the North arm prepared using the cuts described.

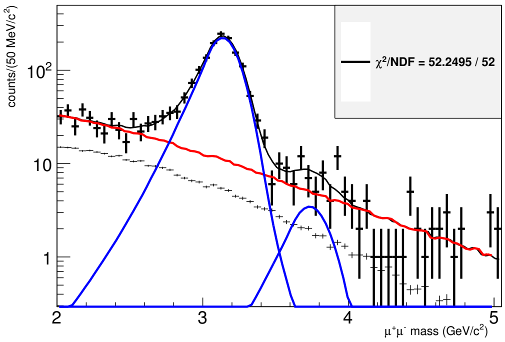

Figure 5: The unlike-sign p+Al dimuon mass spectra for the South arm prepared using the cuts described.

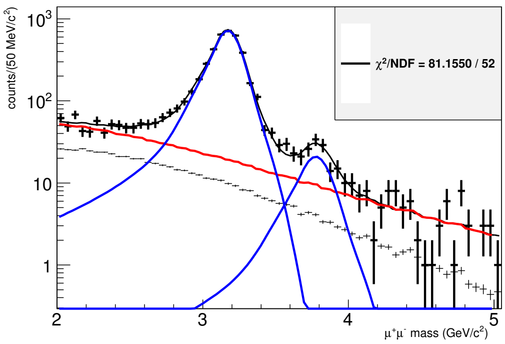

Figure 6: The unlike-sign p+Au dimuon mass spectra for the North arm prepared using the cuts described.

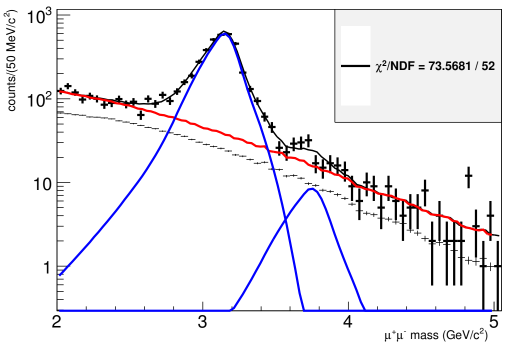

Figure 7: The unlike-sign p+Au dimuon mass spectra for the South arm prepared using the cuts described.

System,Arm	$N_{\psi(1s)}$	$N_{\psi}(2s)$	Corrected $\psi(2s)/\psi(1s)$ ratio
$p+p$, N	6260±156	206±23.4	2.23±0.26%
$p+p$, S	10149±222	294±27.2	1.93±0.18%
p+Al, N	1534±90	42.3±10.9	1.87±0.49%
p+Al, S	1341±121	24.0±11.2	1.19±0.57%
p+Au, N	3914±201	131±17.7	2.27±0.33%
p+Au, S	3417±220	55.2±18.1	1.08±0.36%

Table 3: Number of $\psi(1s)$, $\psi(2s)$, and the corrected ratio of $\psi(2s)/\psi(1s)$, for the p_T integrated dimuon spectra for each system considered in this analysis. Note that there is good agreement on the extracted ratio between the North and South arms in $p+p$, and significant differences between the North and South arms in p+Au.

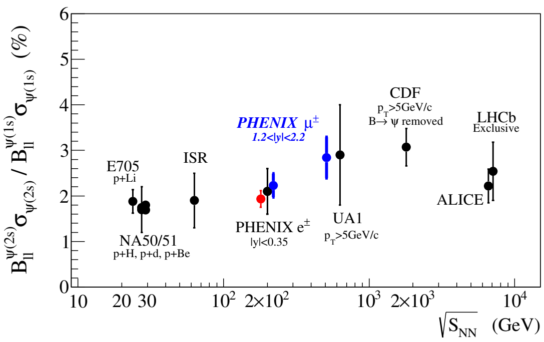

Figure 8: The ratio of inclusive $\psi(2s)/\psi(1s)$ mesons from the Run-15 $p+p$ data, for the North (blue) and South (red) arms, compared to other world data. Only statistical error bars are shown here.

Also of interest is the p_T dependence of the $\psi(2s)/\psi(1s)$ ratio. The mass spectra are divided into several p_T bins and the same fitting procedure is performed. Fits are shown in Figs 10 through 25. Of particular interest is the lowest p_T bin of the p+Au dat in the South arm (p-going direction). The $\psi(2s)$ peak is completely gone, see Fig. 21. The $p+p$ data is shown in p_T bins in Fig 9, which display good agreement within statistical uncertainties between the two muon arms.

I found when doing these fits that the likelihood minimizer prefers a slight negative value on the normalization of the psi prime peak (although, when considering uncertainties, it is consistent with zero). When I constrain the fit to give a non-negative value for the psi prime normalization, the fit will not converge to a minimum that gives reasonable uncertainties on the other fit parameters (e.g., it gives a J/ψ integral that is also consistent with zero, when clearly this cannot be physical). Therefore I let the fit give the number of $\psi(2s)$ mesons that is negative, but consistent with zero and positive values within one σ. On all plots, the one σ upper limit will be shown.

System,Arm	p_T range (GeV/c)	$N_{\psi(1s)}$	$N_\psi(2s)$	Corrected $\psi(2s)/\psi(1s)$ ratio
$p+p$, N	0-1	2014±84	36.2±10.9	1.22±0.37%
$p+p$, S	0-1	3372±108	73.5±14.4	1.46±0.29%
$p+p$, N	1-2	2526±101	85.5±13.2	2.30±0.37%
$p+p$, S	1-2	4031±134	118±17	1.96±0.29%
$p+p$, N	2-3	1165±83	57.6±12	3.34±0.74%
$p+p$, S	2-3	1777±113	71.6±13.2	2.68±0.52%
$p+p$, N	3-4	421.7±66	27.2±7.5	4.35±1.39%
$p+p$, S	3-4	741±76	32.6±9.0	2.94±0.87%
$p+p$, N	4-6	192±25	12.5±3.6	4.41±1.40%
$p+p$, S	4-6	310±62	11.7±6.4	2.56±1.49%
p+Au, N	0-1	1051±88	24.3±8.7	1.56±0.58%
p+Au, S***	0-1	903±107	-5.3±7.7	-0.39±0.57%
p+Au, N	1-2	1526±95	54.2±813.1	2.41±0.60%
p+Au, S	1-2	136±89	21.8±10.9	1.08±0.54%
p+Au, N	2-3	791±63	18.8±7.0	1.61±0.61%
p+Au, S	2-3	706±103	14.9±8.8	1.40±0.86%

Table 4: Number of $\psi(1s)$, $\psi(2s)$, and the corrected ratio of $\psi(2s)/\psi(1s)$, in p_T bins for the $p+p$ and p+Au datasets.

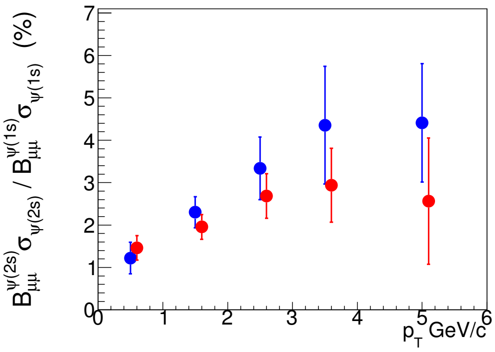

Figure 9: The ratio as a function of p_T for the Run-15 $p+p$ data, as measured by the North arm (blue) and South arm (red). Only statistical uncertainties are plotted here

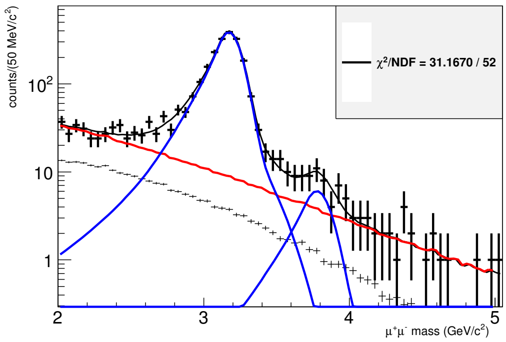

Figure 10: The unlike-sign $p+p$ dimuon mass spectra for the North arm prepared using the cuts described, in the p_T range 0-1 GeV/c.

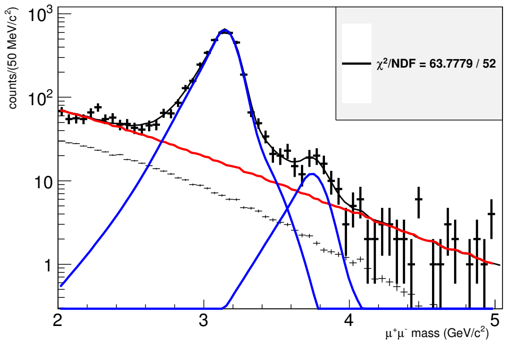

Figure 11: The unlike-sign $p+p$ dimuon mass spectra for the South arm prepared using the cuts described, in the p_T range 0-1 GeV/c.

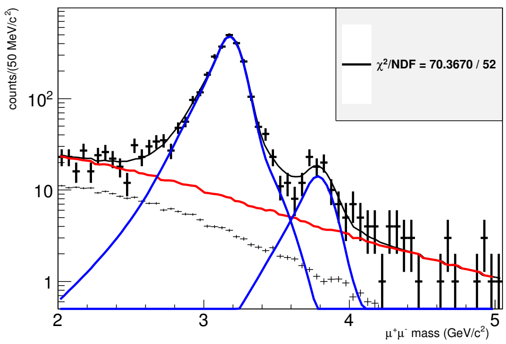

Figure 12: The unlike-sign $p+p$ dimuon mass spectra for the North arm prepared using the cuts described, in the p_T range 1-2 GeV/c.

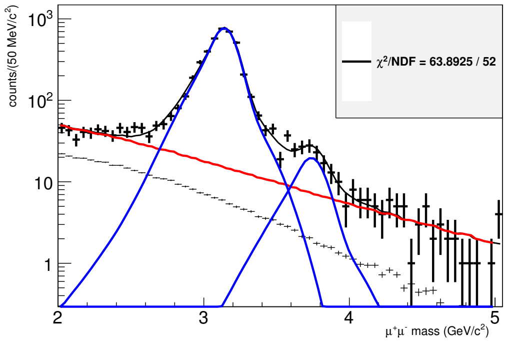

Figure 13: The unlike-sign $p+p$ dimuon mass spectra for the South arm prepared using the cuts described, in the p_T range 1-2 GeV/c.

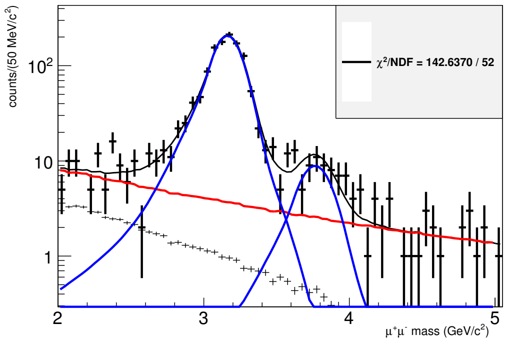

Figure 14: The unlike-sign $p+p$ dimuon mass spectra for the North arm prepared using the cuts described, in the p_T range 2-3 GeV/c.

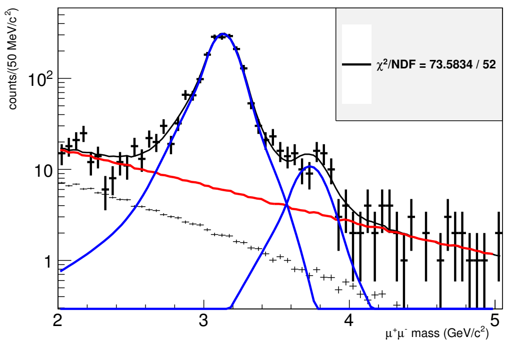

Figure 15: The unlike-sign $p+p$ dimuon mass spectra for the South arm prepared using the cuts described, in the p_T range 2-3 GeV/c.

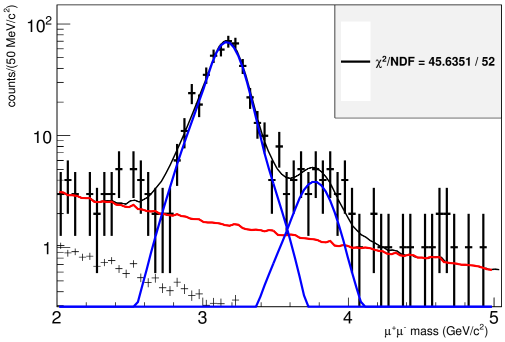

Figure 16: The unlike-sign $p+p$ dimuon mass spectra for the North arm prepared using the cuts described, in the p_T range 3-4 GeV/c.

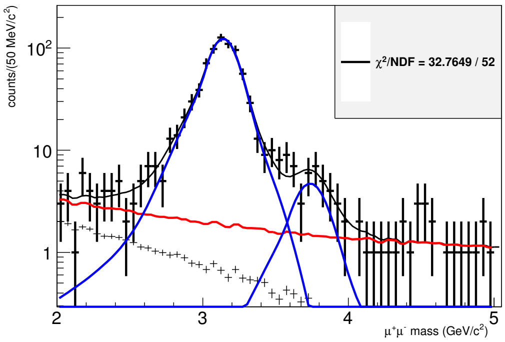

Figure 17: The unlike-sign $p+p$ dimuon mass spectra for the South arm prepared using the cuts described, in the p_T range 3-4 GeV/c.

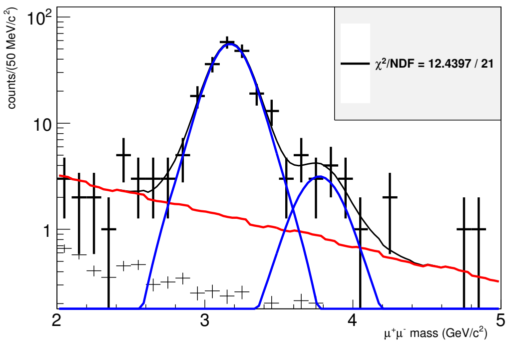

Figure 18: The unlike-sign $p+p$ dimuon mass spectra for the North arm prepared using the cuts described, in the p_T range 4-6 GeV/c.

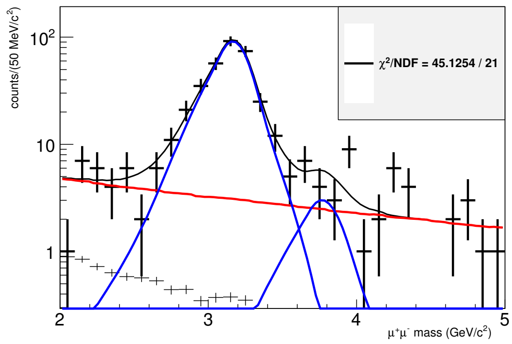

Figure 19: The unlike-sign $p{+}p$ dimuon mass spectra for the South arm prepared using the cuts described, in the p_T range 4-6 GeV/c.

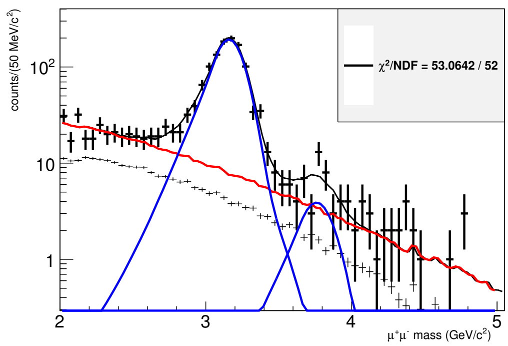

Figure 20: The unlike-sign p+Au dimuon mass spectra for the North arm prepared using the cuts described, in the p_T range 0-1 GeV/c.

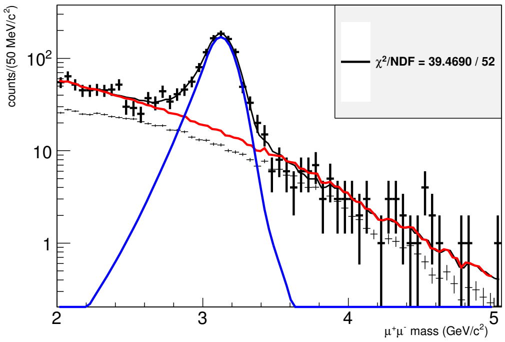

Figure 21: The unlike-sign p+Au dimuon mass spectra for the South arm prepared using the cuts described, in the p_T range 0-1 GeV/c. THIS IS THE INTERESTING ONE.

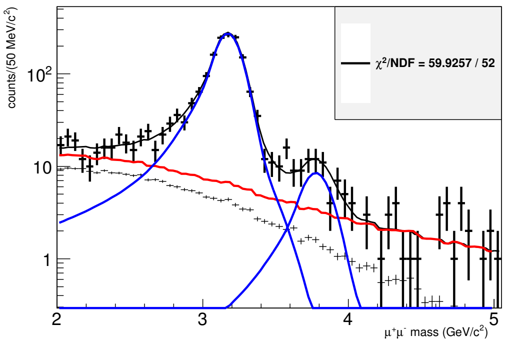

Figure 22: The unlike-sign p+Au dimuon mass spectra for the North arm prepared using the cuts described, in the p_T range 1-2 GeV/c.

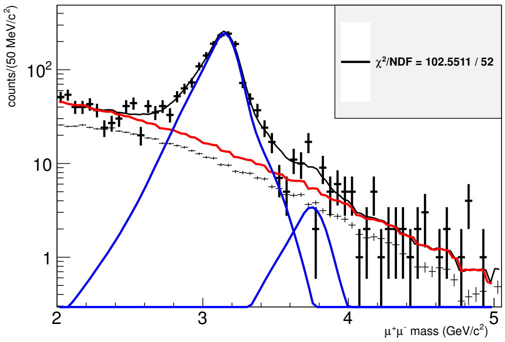

Figure 23: The unlike-sign p+Au dimuon mass spectra for the South arm prepared using the cuts described, in the p_T range 1-2 GeV/c.

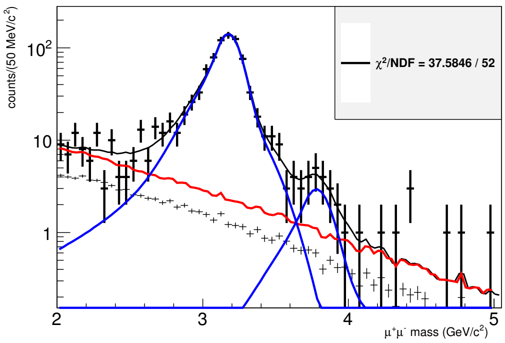

Figure 24: The unlike-sign p+Au dimuon mass spectra for the North arm prepared using the cuts described, in the p_T range 2-3 GeV/c.

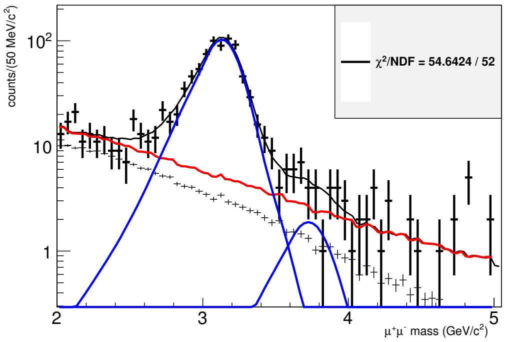

Figure 25: The unlike-sign p+Au dimuon mass spectra for the South arm prepared using the cuts described, in the p_T range 2-3 GeV/c.

6 Systematic Uncertainty Evaluation

Here the various systematic uncertainties assigned to the peak yields and ratios are described.

As previously described, there are two constraints on the fitting function used to determine the peak yields. First we will look at the constraint on the width of the $\psi(2s)$ peak. For the central value it is constrained to be 1.15 times the width of the $\psi(1s)$ peak. To determine a systematic uncertainly due to this constraint, the peak width is varied down to 1.10 and up to 1.20 times the $\psi(1s)$ peak width, and the ratio is re-extracted. The results of this procedure are summarized in Table 5. A systematic uncertainty of 3% is assigned to the ratio due to this constraint.

System,Arm	Ratio of 2s to 1s width	Corrected $\psi(2s)/\psi(1s)$ ratio	Deviation from central value
$p+p$, N	1.2	2.29±0.25%	2.6%
$p+p$, S	1.2	1.98±0.19%	2.6%
$p+p$, N	1.1	2.16±0.25%	3.1%
$p+p$, S	1.1	1.88±0.18%	2.6%
p+Au, N	1.2	2.08±0.32%	2.4%
p+Au, S	1.2	0.89±0.37%	1.3%
p+Au, N	1.1	1.99±0.30%	2.0%
p+Au, S	1.1	0.86±0.35%	2.1%

Table 5: Summary of changes in the ratio of $\psi(2s)/\psi(1s)$ when adjusting the fit constraint on the width of $\psi(2s)$ peak from its central value of 1.15. A systematic uncertainty of 3% is assigned.

The other constraint on the fit is the width of the second Gaussian that is included in each peak. Previous studies have shown that this peak is likely due to tracks which are poorly reconstructed in the muon trackers. However, simply excluding all these tracks gives an undesirable loss of statistics. Selecting only these tracks gives a $\psi(1s)$ width near 200 MeV. Therefore, the width of the second Gaussian is set to 200 MeV in the fitting routine. A systematic uncertainty is determined by varying this peak width between 150 and 250 MeV and repeating the fits. A summary of the changes in the ratio due to the variation of this width is shown in Table 6. This is the dominant systematic uncertainty on this measurement. A systematic uncertainty of 13% is assigned to this ratio for the $p+p$ data and the North arm p+A data, with 25% assigned to the South arm p+A data.

System,Arm	Second Gaussian width	Corrected $\psi(2s)/\psi(1s)$ ratio	Deviation from central value
$p+p$, N	250	2.0±0.25%	12%
$p+p$, S	250	1.66±0.19%	14%
$p+p$, N	150	2.46±0.26%	10%
$p+p$, S	150	2.22±0.2%	15%
p+Au, N	250	1.80±0.32%	13%
p+Au, S	250	0.66±0.36%	25%
p+Au, N	150	2.27±0.33%	11%
p+Au, S	150	1.08±0.36%	23%

Table 6: Summary of changes in the ratio of $\psi(2s)/\psi(1s)$ when adjusting the fit constraint on the width of the second Gaussian peak from its central value of 200 MeV.

The mass range over which the mixed-event combinatorial background is normalized to the like-sign dimuon spectrum may also affect the peak yields. In the nominal case, the mass range is 2-5 GeV. This range is varied to include the ranges 1.5-5 GeV and 2.5-5.5 GeV. The changes in the extracted ratios are summarized in Table 7. The systematic uncertainties assigned due to this effect are 1.5% for the $p+p$ and North arm p+A data, and 12% for the South arm p+A data (note that this is the A-going direction, where combinatorial background is highest, so it is not surprising that this is a larger effect here).

System,Arm	Mass range for normalization (GeV)	Corrected $\psi(2s)/\psi(1s)$ ratio	Deviation from central value
$p+p$, N	1.5-5	2.26±0.44%	1.3%
$p+p$, S	1.5-5	1.99±0.19%	3.1%
$p+p$, N	2.5-5.5	2.22±0.25%	0.5%
$p+p$, S	2.5-5.5	1.91±0.19%	1%
p+Au, N	1.5-5	2.00±0.31%	1.1%
p+Au, S	1.5-5	0.73±0.33%	17%
p+Au, N	2.5-5.5	2.05±0.32%	1%
p+Au, S	2.5-5.5	0.94±0.35%	7%

Table 7: Summary of changes in the ratio of $\psi(2s)/\psi(1s)$ when adjusting the range over which the mixed event background is normalized.

Other systematic uncertainties come from the uncertainty on the ratio of the values of the acc $\times$ efficiency correction at the $\psi(2s)$ and $\psi(1s)$ peaks that are used to correct the measured ratio. As previously discussed, this preliminary analysis is using the relative correction found from the Run-13 preliminary analysis. That was assigned an uncertainty of 1%. To be conservative, that uncertainty is doubled here, to 2%. Similarly, we double the uncertainty on the trigger efficiency correction form 2.5% to 5%. A summary of all systematic uncertainties on the ratio $\psi(2s)/\psi(1s)$ is given in Table 8.

Uncertainty Source	$p+p$	p+A North arm (p-going)	p+A South arm (A-going)
$\psi(2s)$ width constraint	3%	3%	3%
Second Gaussian width constraint	13%	13%	25%
Mixed event mass range normalization	1.5%	1.5%	12%
Relative acc$\times$eff correction	2%	2%	2%
Relative trigger efficiency	5%	5%	5%
TOTAL	14%	14%	28%

Table 8: Summary of systematic uncertainties on the $\psi(2s)/\psi(1s)$ ratio.

A physics quantity where many uncertainties may cancel is the double ratio between pA and pp, defined as $[\psi(2s)/\psi(1s)]_{pA}/[\psi(2s)/\psi(1s)]_{pp}$. To determine the extent to which these uncertainties cancel, the double ratio was re-calculated for each of the above cases where the fitting procedure was varied. The results are given in Table 9. Given the results in this table, for each of the sources of systematic uncertainty, we take the deviation in the central value for the upper and lower extremes and average it for each arm independently. The three terms are added in quadrature to find the total systematic uncertainty on the double ratio. For the N arm, this comes out to 11%, and for the South arm, 29%.

Uncertainty Source	Resulting double ratio	Deviation from central value
$\psi(2s)$ width constraint increased, N arm	0.99	7%
$\psi(2s)$ width constraint decreased, N arm	1.01	5%
$\psi(2s)$ width constraint increased, S arm	0.42	16%
$\psi(2s)$ width constraint decreased, S arm	0.44	14%
Second Gaussian width increased, N arm	1.01	5%
Second Gaussian width decreased, N arm	0.98	8%
Second Gaussian width increased, S arm	0.37	27%
Second Gaussian width decreased, S arm	0.47	8%
Mixed event mass range lowered, N arm	0.98	7%
Mixed event mass range raised, N arm	1.01	5%
Mixed event mass range lowered, S arm	0.36	29%
Mixed event mass range raised, S arm	0.46	8%

Table 9: Summary of systematic uncertainties on the double ratio $[\psi(2s)/\psi(1s)]_{pA}/[\psi(2s)/\psi(1s)]_{pp}$.

7 Results

For all $p + p$ data, the North and South arms are averaged together following the procedure the PDG uses for combining different measurements of the same quantity. This gives a value of 2.13±0.15(stat) ±0.30(sys) for the ratio of inclusive $\psi(s2)/\psi(1s)$. The statistical and systematic uncertainties are combined in quadrature and the data is plotted along with world data in Fig. 26

The same procedure is done bin-by-bin for the p_T dependent ratio. The results are shown in Fig. 27.

The p_T integrated double ratio is shown in Fig. 28. The error bars (boxes) on the points represent the statistical (systematic) uncertainties on the double ratio from the p+A data only. Since all the forward and backward rapidity points have a common $p + p$ reference, the uncertainties from this $p + p$ denominator are added in quadrature and quoted as the 15.6% global uncertainty in text on the plot. The midrapidity point is from PPG151.

The p_T dependent double ratio from the p+Au data is shown in Fig. 29. This is how I calculated the upper bound for the one point:

When I let the likelihood fitter find a minimum, it prefers a slightly negative value for the number of $\psi(2s)$, that is consistent with zero. From Table 4, we see that the fit wants to give me -5.3±7.7 counts in the $\psi(2s)$ peak, with a corresponding corrected ratio of -0.39±0.57%. This gives a relative statistical uncertainty of 1.46. I add that in quadrature with the South arm double ratio systematic uncertainty of 29% that is described in the previous section, for a total relative uncertainty of 1.49, which makes the single ratio come out to -0.39±0.58. Dividing by the ratio for that p_T bin in $p + p$, 1.37, gives me a double ratio value of -0.285±0.42. Going one σ up from the central value of this quantity gives 0.135, rounded up to 0.14. I put the top of the arrow there and, since a negative value for the amount of $\psi(2s)$ mesons we counted is not physical, extend the arrow down to zero and call this a one σ upper limit.

The yellow boxes in each p_T bin represent the uncertainty on the $p + p$ denominator for that bin.

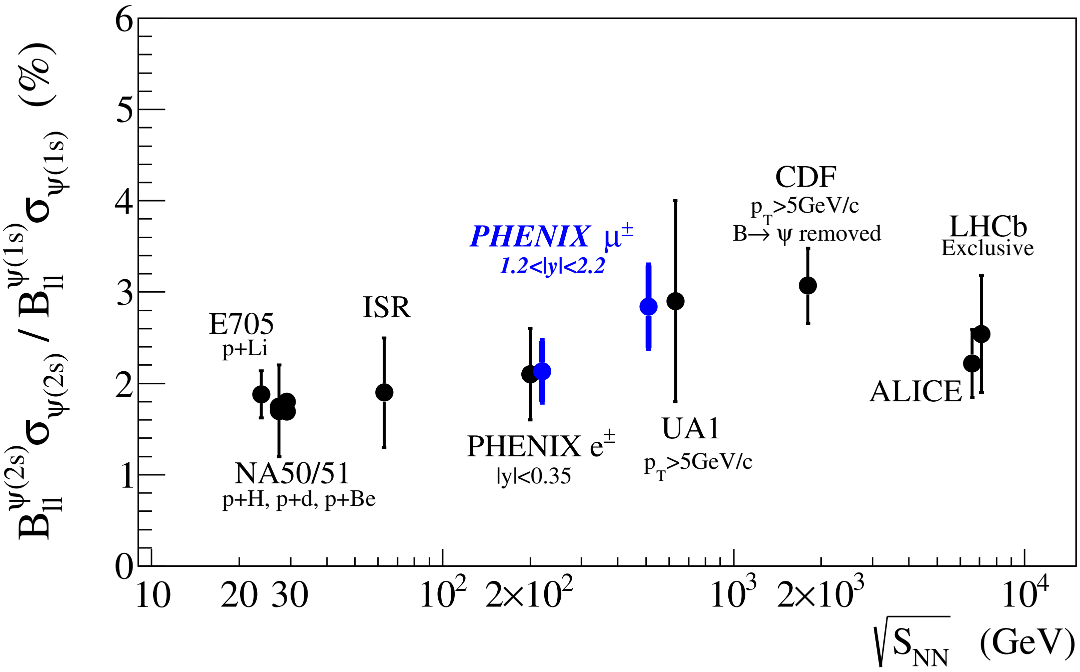

Figure 26: The combined N and S ratio for the $p + p$ data, compared to world data.

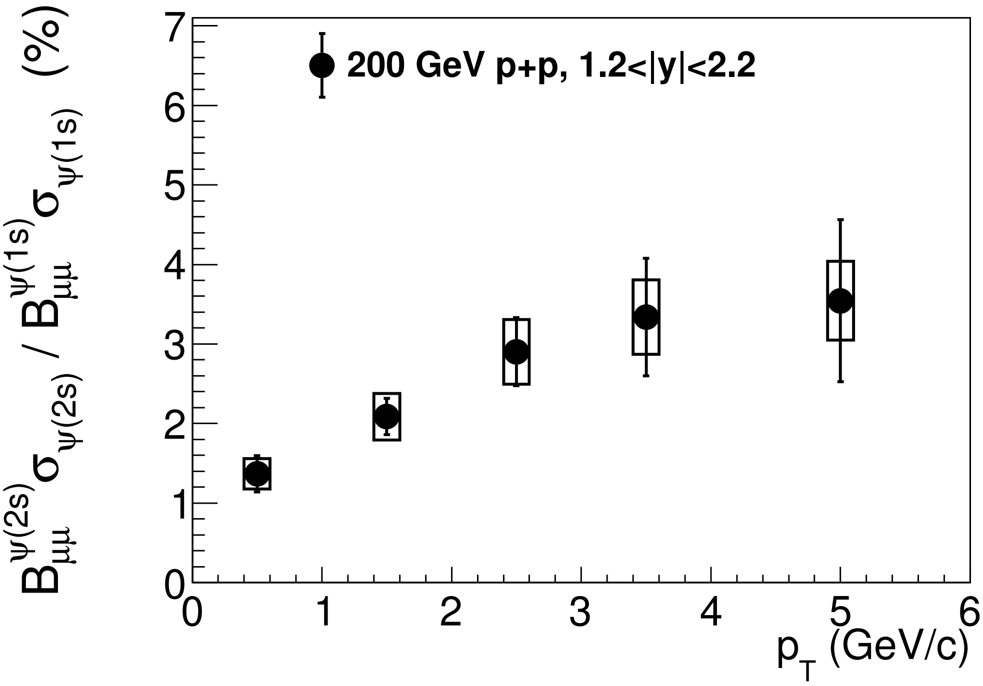

Figure 27: The combined N and S ratio for the $p + p$ data as a function of p_T.

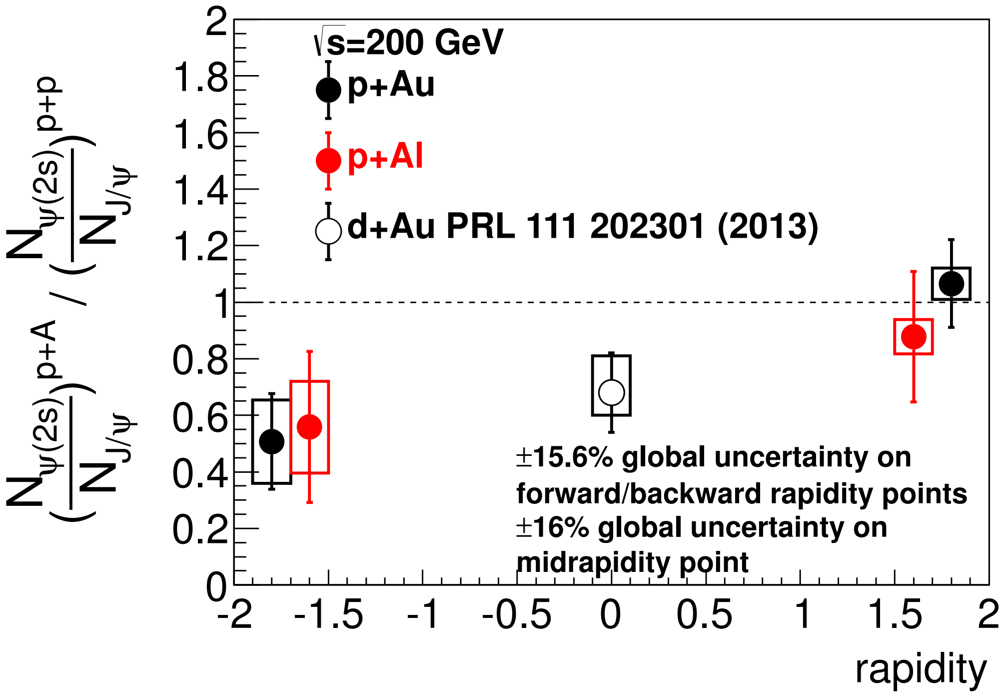

Figure 28: The double ratio, shown along with the central arm data point from PPG151.

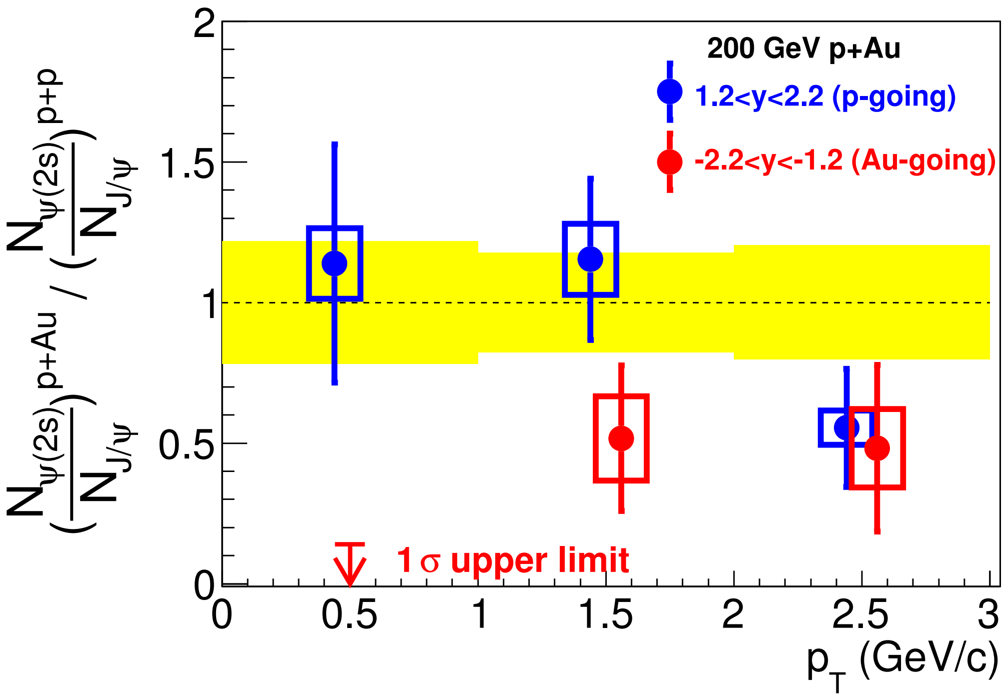

Figure 29: The double ratio divided into momentum bins.